Optical nanotrapping using cloaking metamaterial

Edward P. Furlani* and Alexander Baev
The Institute for Lasers, Photonics and Biophotonics, State University of New York at Buffalo, Buffalo, New York 14260, USA
(Received 26 December 2007; revised manuscript received 8 December 2008; published 19 February 2009)

We study the electromagnetic behavior of spherical semishell structures that have cloaking material properties proposed by Pendry, Schurig, and Smith [Science **312**, 1780 (2006)]. We use three-dimensional full-wave time-harmonic field analysis to evaluate the field and dipolar force distribution produced by these structures in free-space under plane wave illumination. We show that the optical force in proximity to these structures is suitable for active and size-selective manipulation and trapping of neutral nanoscale particles.

DOI: 10.1103/PhysRevE.79.026607 PACS number(s): 41.20.Jb, 42.60.Da, 42.25.Bs, 42.25.Fx

I. INTRODUCTION

Recently, Pendry *et al.* have proposed a method for designing media that can be used to electromagnetically "cloak" a region [1]. The cloaking material properties are derived from a coordinate transformation that mathematically "squeezes" the cloaked region into a surrounding shell structure. This transformation is mapped to tensor-valued permittivity and permeability properties that are both anisotropic and spatially varying. These properties apply to the shell only, which acts as an electromagnetic shield for both its interior and exterior domains; i.e., the inner domain is shielded from external irradiation, while the outer domain is simultaneously shielded from fields generated within. The ability to cloak a region using custom tailored media has attracted substantial interest, especially as it holds unique potential for applications such as stealth technology. Furthermore, the development of such media has benefited from advances in the field of metamaterials [2–12]. Specifically, a crude cloaking system has been demonstrated at microwave frequencies using artificially structured materials [13].

To date, almost all research on cloaking media has focused on the analysis of fully cloaked cylindrical and spherical regions [14–19]. However, we recently studied incomplete cloaking metamaterial shells with apertures, and found that they formed resonant cavities that can be excited using plane wave illumination [20]. We continue this work and present a study of the electromagnetic behavior of cloaking metamaterial spherical semishell structures in free space. We show that these structures can be used for optical manipulation and trapping of neutral (dielectric) nanoparticles.

The interest in optical manipulation and trapping continues to grow, especially for biological applications where the manipulated objects include viruses, cells, and intracellular organelles [21–25]. While micron and submicron particles can be manipulated using conventional laser tweezers, the resolution of this approach is diffraction limited (~250 nm), and the high optical power and focusing of the laser beam can limit the exposure time of a trapped specimen. An alternate trapping method that overcomes these limitations involves the use of plasmonics [26–32]. Specifically, subwavelength particles can be manipulated and trapped using the enhanced near-field gradients that exist around illuminated metallic nanostructures. In this paper we show that spherical semishells of cloaking metamaterial provide still another alternative for implementing nanoscale optical manipulation and trapping (Fig. 1). We use three–dimensional (3D) full-wave time-harmonic finite element analysis (FEA) to study the field, power flow, and dipolar force distribution of such structures under plane wave illumination at optical frequencies. We show that the field bending behavior of these structures produce local field enhancement and field gradients that give rise to an optical dipolar force that is sufficient to trap dielectric nanoparticles. We show that these results hold for lossy metamterials as well.

II. THEORY

In this section we first review the material properties of spherical cloaking shell structures, and then discuss the method we use for computing optical forces on dielectric particles. Consider a spherical shell that is centered at the origin. Let the inner and outer radii of the shell be denoted by R_1 and R_2, respectively. Following Pendry, Schurig, and Smith [1], we apply the following coordinate transformation that "squeezes" the entire spherical region $0 \leqslant r < R_2$ into the annulus $R_1 < r < R_2$:

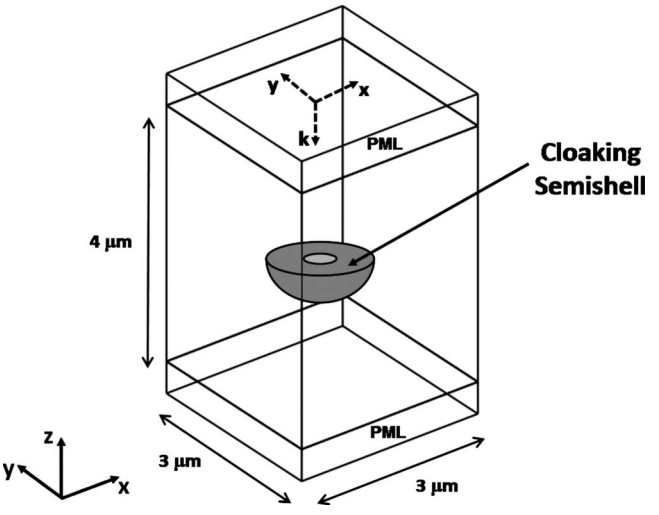

FIG. 1. Semishell of cloaking material in the computational domain.

*efurlani@buffalo.edu

$$r' = R_1 + \frac{(R_2 - R_1)}{R_2} r,$$

$$\theta' = \theta,$$

$$\phi' = \phi. \tag{1}$$

This transformation is mapped to "cloaking" permittivity and permeability material tensors $\bar{\bar{\varepsilon}}_c$ and $\bar{\bar{\mu}}_c$,

$$\bar{\bar{\varepsilon}}_c = \bar{\bar{\mu}}_c = \frac{R_2}{R_2 - R_1}\left(\frac{r - R_1}{r}\right)^2 \hat{\mathbf{r}}\hat{\mathbf{r}} + \frac{R_2}{R_2 - R_1}\hat{\boldsymbol{\theta}}\hat{\boldsymbol{\theta}} + \frac{R_2}{R_2 - R_1}\hat{\boldsymbol{\phi}}\hat{\boldsymbol{\phi}}, \tag{2}$$

where $0 \leqslant \theta \leqslant \pi$, $0 \leqslant \phi \leqslant 2\pi$, and $\hat{r}$, $\hat{\theta}$, $\hat{\phi}$ are unit vectors in spherical coordinates [1]. For the numerical analysis, we convert these tensors to Cartesian components

$$\bar{\bar{\varepsilon}}_c = \frac{R_2}{R_2 - R_1}\begin{bmatrix} 1 + \gamma(r)\cos^2(\phi)\sin^2(\theta) & \gamma(r)\sin(\phi)\cos(\phi)\sin^2(\theta) & \gamma(r)\cos(\phi)\sin(\theta)\cos(\theta) \\ \gamma(r)\sin(\phi)\cos(\phi)\sin^2(\theta) & \beta(r)\sin^2(\phi) + \cos^2(\phi) - \gamma(r)\cos^2(\theta)\sin^2(\phi) & \gamma(r)\sin(\phi)\sin(\theta)\cos(\theta) \\ \gamma(r)\cos(\phi)\sin(\theta)\cos(\theta) & \gamma(r)\sin(\phi)\sin(\theta)\cos(\theta) & 1 + \gamma(r)\cos^2(\theta) \end{bmatrix}, \tag{3}$$

where $\beta(r) = (\frac{r - R_1}{r})^2$ and $\gamma(r) = \beta(r) - 1$. Note that Eq. (3) gives the Cartesian components of the relative material tensors in terms of the spherical coordinates (r, θ, ϕ), i.e., $\varepsilon_{xx} = \frac{R_2}{(R_2 - R_1)}[1 + \gamma(r)\cos^2(\phi)\sin^2(\theta)]$. To analyze a cloaked sphere $(r < R_1)$, we solve Maxwell's equations using the constitutive relations

$$\bar{\bar{\varepsilon}} = \bar{\bar{\mu}} = \begin{cases} I, & r < R_1 \text{ and } r > R_2, \\ \bar{\bar{\varepsilon}}_c, & R_1 < r < R_2, \end{cases} \tag{4}$$

where I is the 3×3 identity matrix.

We analyze the optical trapping of sub-wavelength particles by computing the time-averaged dipolar force

$$\langle F_i \rangle = \frac{1}{2}\sum_j \mathrm{Re}[\alpha E_{0j} \partial^i (E_{0j})^*], \tag{5}$$

where E_{0j} $(j = 1, 2, 3)$ are the Cartesian components of the optical field and

$$\alpha = \frac{4\pi\alpha_0\varepsilon_0}{\left[1 - \alpha_0\left(\frac{k^2}{R_p} - \frac{2}{3}ik^3\right)\right]} \tag{6}$$

is the polarizability of the particle, where $\alpha_0 = R_p^3(\varepsilon_r - 1)/(\varepsilon_r + 2)$. R_p and ε_p are the radius and relative permittivity of the particle, respectively. The optical force consists of two components, a scattering force and a gradient force. The imaginary term in α accounts for the scattering force. It is important to note that the sign of this term (i.e., $\pm\frac{2}{3}ik^3$) depends on the convention used in the time-harmonic analysis, i.e., $\exp(\pm i\omega t)$ [33–35]. We use the COMSOL high-frequency EM solver for our analysis, which employs the $\exp(i\omega t)$ convention and is compatible with Eq. (6).

III. RESULTS AND DISCUSSION

We begin our study with an analysis of a spherical shell of cloaking metamaterial. We verify the performance of the cloaking material properties in Eq. (3) via simulation. As noted above, we use the COMSOL Multiphysics FEA-based electromagnetic solver for our numerical analysis. The computational domain spans 5 μm in the direction of propagation (z axis), and 3 μm in both the x and y directions (Fig. 1). The cloaking shell has inner and out radii $R_1 = 200$ and $R_2 = 600$ nm, respectively, and is centered at the origin in the computational domain (Fig. 2). We apply perfectly matched layers (PMLs) at the top and bottom of the computational domain to reduce backscatter at these boundaries. The PMLs are 0.5 μm in height, which leaves 4 μm of physical domain along the z axis. We impose perfect electric conductor conditions at the boundaries perpendicular to the E field at $x = \pm 1.5$ μm, and perfect magnetic conductor conditions at the boundaries perpendicular to the H field at $y = \pm 1.5$ μm. These symmetry boundary conditions ensure normal incidence of the respective fields at the boundaries transverse to the direction of propagation, and they mimic a two–dimensional (2D) array of spherical shells with a center-to-center lattice spacing of 3 μm in both the x and y directions. Thus, we are studying the field due to a single element of a 2D array of spherical cloaking shells.

We illuminate the spherical shell with a downward directed uniform TEM plane wave with the E field along the x axis. The incident field is generated by a time-harmonic ($\lambda = 800$ nm) surface current source positioned in the x-y plane 2 μm above the top surface of the semishell, i.e., at $z = 2$ μm (immediately below the upper PML). The magnitude of the surface current is chosen to provide a plane wave with a field magnitude of $E_x = 2 \times 10^6$ V/m, which corresponds to an incident intensity of 5.29×10^9 W/m^2. The numerical FEA model comprised 16 000 cubic vector elements with 306 000 degrees of freedom. The full-wave analysis shown in Fig. 2 demonstrates that the Cartesian material properties in Eq. (3) render the interior of the shell cloaked, as expected. Specifically, an ideal cloaking metamaterial bends and focuses the incident EM wave in a unique way so as to shield its interior from the wave without reflection or loss. In this regard, note from Figs. 2(a) and 2(b) that the field is enhanced inside the shell but not outside. Specifically, inside

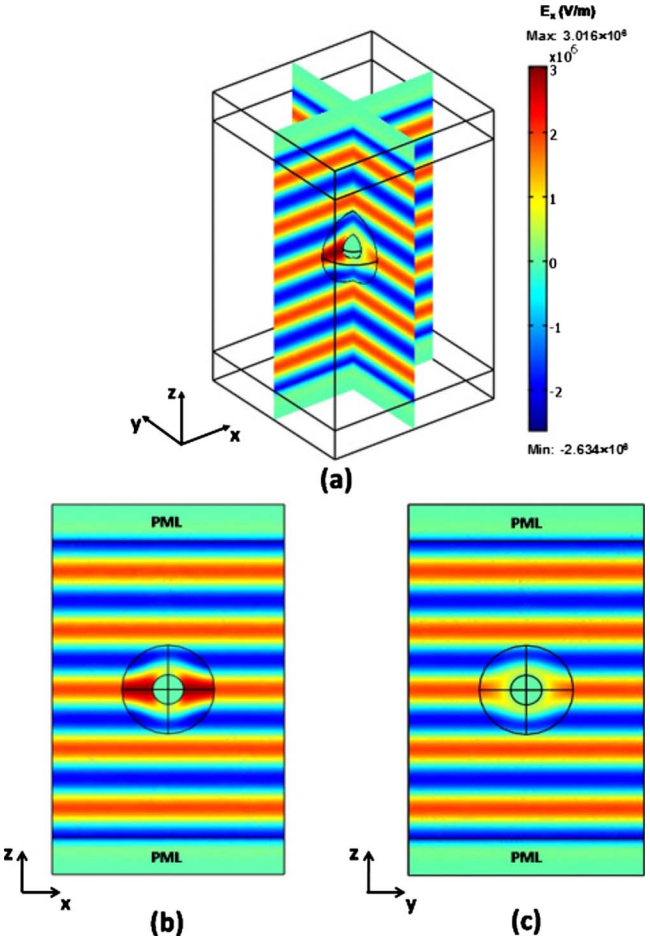

FIG. 2. (Color online) Full-wave 3D time-harmonic field analysis for cloaked sphere ($\lambda=800$ nm): (a) E_x in two orthogonal planes showing a cloaked core ($r<R_1$), (b) E_x in the x-z plane, and (c) E_x in the y-z plane.

the shell a peak field value of $E_x=3\times10^6$ V/m is observed, whereas outside, the unperturbed free-space magnitude is $E_x=2\times10^6$ V/m.

Next, we study a semishell of cloaking metamaterial as shown in Fig. 1. All parameters and boundary conditions are as above. However, instead of using a current source to generate the incident field we employ a scattering field analysis. We specify a time-harmonic ($\lambda=800$ nm) incident field with a magnitude of $E_x=2\times10^6$ V/m. The cloaking material properties in Eq. (3) are applied to the semishell only; all other regions are assumed to be free space. The FEA model for this geometry consisted of 23 285 cubic vector elements with 422 233 degrees of freedom.

A plot of the negative time-averaged electric energy density $-\langle W_e\rangle$ at 1100 nm above the shell is shown in Fig. 3(a). This function is proportional to the dipolar gradient force potential, i.e., $\langle W_e\rangle=\frac{1}{4}\varepsilon_0\mathrm{Re}(\mathbf{E}\cdot\mathbf{E})$, and we use it to identify potential regions of particle trapping. Specifically, the plot in Fig. 3(a) exhibits a central minimum, which implies particle trapping or confinement in this plane, i.e., the lateral optical forces act to keep a dielectric particle near the z axis. We explore this in more detail below. A cross-sectional plot of the total (incident plus scattered) x-directed field component E_x in the y-z plane is shown in Fig. 3(b). From this plot we find that the E field in locally enhanced by the presence of the semishell at various regions of the computational domain, i.e., the maximum observed field is $E_x=2.699\times10^6$ V/m, whereas the unperturbed free-space magnitude is $E_x=2\times10^6$ V/m. This is due to the EM bending and focusing nature of the semishell, which acts to deform the field (see also Fig. 4). The induced spatial field variation results in localized field gradients that give rise to a dipolar force. We confirm this by computing the time-averaged axial dipolar force F_z on nanoparticles along the z axis. We assume that all particles have a relative dielectric permittivity $\varepsilon_p=2.25$. We compute F_z for different sized nanoparticles $R_p=50$, 75, 100, and 125 nm [Fig. 3(c)]. Axial trapping points occur where F_z changes sign, i.e., from positive below the point to negative above it. Thus, below the point F_z acts to move the particle upward, whereas above the point F_z acts to move the particle downward. In Fig. 3(c) we identify two such points near $z=1100$ nm, one for $R_p=100$ nm and another for $R_p=125$ nm. From this analysis, we find that the trapping position depends of the particle size. Thus, a semishell metamaterial structure could potentially be used for size selective nanoparticle separation. It should also be noted that larger particles are not necessarily trapped as their free-space scattering force, which acts downward in the direction of propagation of the incident field, can exceed their gradient force.

It is instructive to compare the time-averaged power flow vectors in the y-z plane for the spherical shell and the semishell geometries (Fig. 4). In the former, the power flow is uniform outside the sphere as is the field, and there is no gradient force. However, as noted above, the semishell distorts the power flow and field throughout the computational domain, thereby producing local field gradients that give rise to regions of particle trapping.

We also plot time-averaged force vectors along with $-\langle W_e\rangle$, which is proportional to the gradient force potential, in the y-z plane for the semishell structure (Fig. 5). We identify a trapping region near $z=1100$ nm using a dotted circle that has a diameter equal to the wavelength of the incident light $\lambda=800$ nm. Note that the trapping region is subwavelength. The trapping force in this region exceeds both the gravitational force as well as the Langevin force, which we estimate at $T=300$ K in air with the measurement period of 1 s. Another way to evaluate the viability of particle trapping against Brownian motion is to compare the trapping potential $U_{\mathrm{trap}}=-\pi\varepsilon_0R_p^3[(\varepsilon_r-1)/(\varepsilon_r+2)]\mathrm{Re}(\mathbf{E}\cdot\mathbf{E})$ with the Brownian energy k_BT. At room temperature of 300 K the Brownian energy is 4.14×10^{-21} J. The magnitude of the trapping potential for our system can be estimated from the plot of the time-averaged electric energy density $\langle W_e\rangle=\frac{1}{4}\varepsilon_0\mathrm{Re}(\mathbf{E}\cdot\mathbf{E})$ by multiplying this quantity within the trap, where it is relatively flat, by $4\pi R_p^3[(\varepsilon_r-1)/(\varepsilon_r+2)]$ [see Eqs. (5) and (6)]. For example, $\langle W_e\rangle=16.75$ J/m^3 in the center of the trapping region at $z=1100$ nm (Fig. 5). Therefore, for a dielectric particle ($\varepsilon_r=2.25$) with $R_p=100$ nm, the magnitude of the trapping potential is 6.19×10^{-20} J, which is more than an order of magnitude greater than the thermal energy. Moreover, based on this first-order analysis, we estimate that particles with a radius greater than 40 nm can be trapped with the given incident intensity of 5.29×10^9 W/m^2. Smaller par-

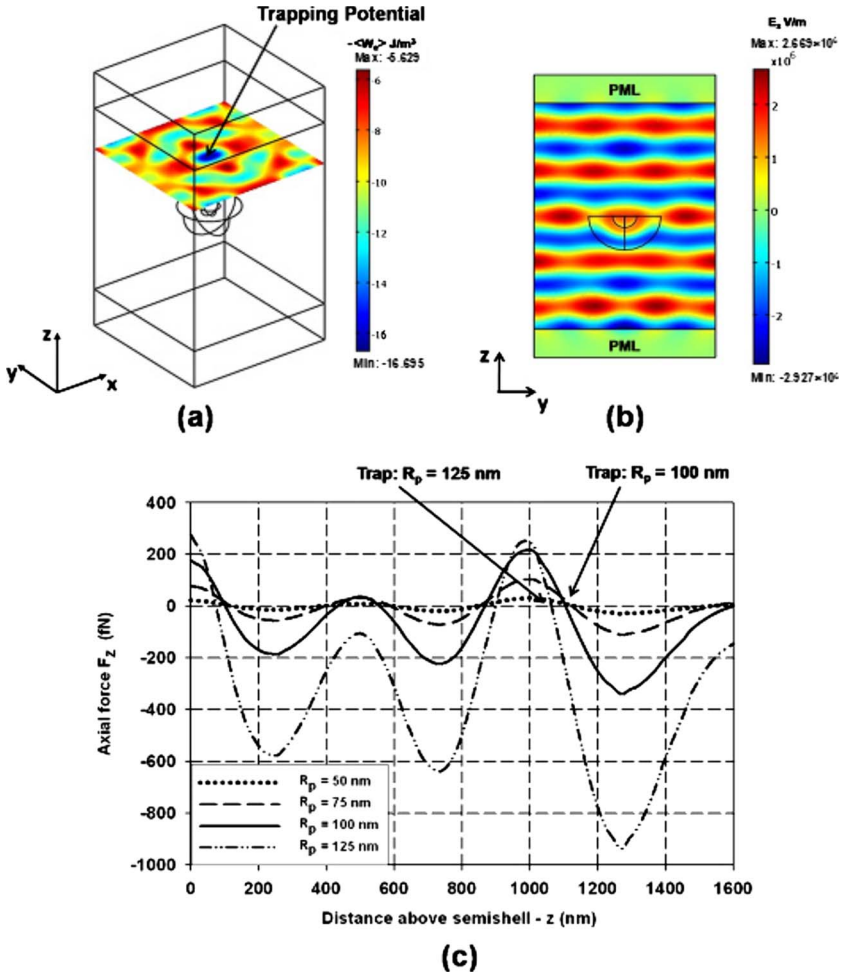

FIG. 3. (Color online) TEM full-wave analysis of semishell of cloaking metamaterial ($\lambda = 800$ nm): (a) time-averaged electric energy density $-\langle W_e \rangle$ in the x-y plane 1100 nm above the semishell, (b) E_x in the y-z plane, and (c) axial dipolar force F_z along the z axis above the semishell as a function of particle radius R_p.

ticles can be trapped by increasing the intensity. These results are similar to those obtained using plasmonic-based nanotrapping where it was estimated that polystyrene nanoparticles with a radius greater than 27 nm could be trapped using an incident intensity of 10^{11} W/m^2 [28]. Thus, cloaking metamaterial-based nanotrapping has performance that is comparable to, and potentially exceeds, that of plasmonic-

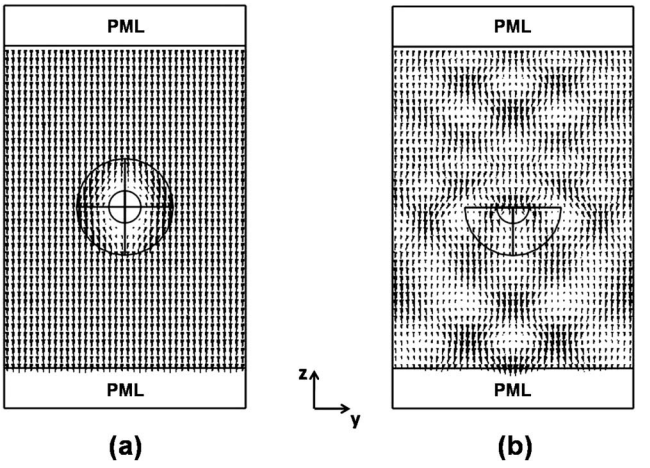

FIG. 4. Tine-averaged power flow vectors in the y-z plane ($\lambda = 800$ nm): (a) cloaked sphere and (b) semishell of cloaking metamaterial.

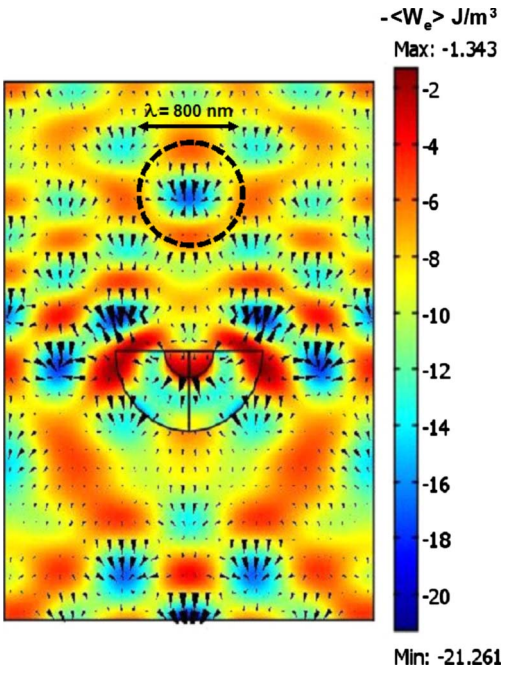

FIG. 5. (Color online) Time-averaged dipolar force on a dielectric particle ($R_p = 100$ nm), and the time averaged electric energy density $-\langle W_e \rangle$ in the y-z plane for $\lambda = 800$ nm (dotted circle indicates a trapping region).

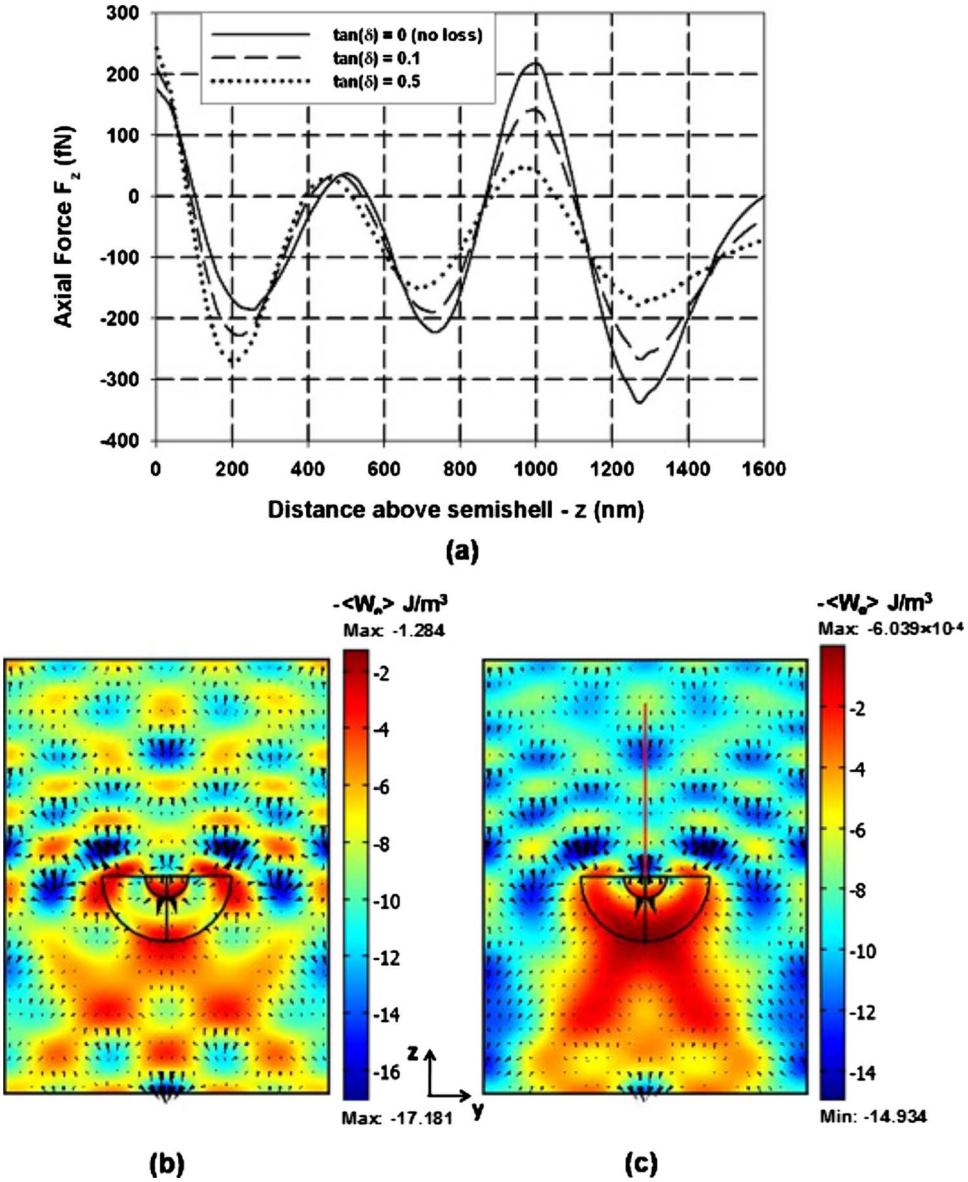

FIG. 6. (Color online) TEM full-wave analysis of the semishell of lossy cloaking metamaterial ($\lambda = 800$ nm, $R_p = 100$ nm): (a) axial dipolar force F_z along the z axis above the semishell as a function of loss tangent introduced into each component of the permittivity and permeability tensors, (b) time-averaged electric energy density $-\langle W_e \rangle$ in the y-z plane for $\tan(\delta) = 0.1$, and (c) time-averaged electric energy density $-\langle W_e \rangle$ in the y-z plane for $\tan(\delta) = 0.5$.

based nanotrapping. It offers an additional potential advantage in that metamaterial semishells can in principle be designed for trapping at an arbitrary specified wavelength, as opposed to natural (e.g., metallic) materials that have a more limited resonant response to free-space illumination.

Last, we study the performance of a lossy semishell of metamaterial [17,18,36]. Specifically, we introduce a loss term into each component of the permittivity and permeability tensors, and then recompute the field and force distribution of the semishell defined above [16,36]. We choose two different values for the loss tangent, $\tan(\delta) = 0.1$ and 0.5, respectively. In Fig. 6(a), we compare the axial force on a nanoparticle ($R_p = 100$ nm, $\varepsilon_p = 2.25$), with and without loss. Note that the shape of the force profile is similar in both cases, but the magnitude of the force decreases as loss increases and there is a shift in the trapping position. A plot of the time-averaged force and $-\langle W_e \rangle$ in the y-z plane for $\tan(\delta) = 0.1$ and 0.5 are shown in Figs. 6(b) and 6(c), respectively. It is instructive to compare these with a similar plot for the lossless material, which is shown in Fig. 5. We find that as loss increases, the field focusing of the semishell decreases as does the trapping force.

IV. CONCLUSIONS

We have used full-wave time-harmonic analysis to study the optical field, power flow, and dipolar force distribution produced by spherical semishells of cloaking metamaterial in free-space under plane wave illumination. We have shown that the EM bending nature of the structures produce local field enhancement and field gradients that give rise to forces on dielectric particles. The induced optical forces are sufficient to manipulate and trap neutral nanoscale particles, and the strength and location of the trap depend on the particle size. We have also shown that these results hold for lossy metamaterials as well. Thus, the semishell structures could potentially be used for active size-selective nanoparticle separation. Moreover, cloaking metamaterial-based nanotrapping has performance that is comparable to, and

potentially exceeds, that of plasmonic-based nanotrapping. It has a potential advantage in that cloaking metamaterials semishells can, in principle, be designed for trapping at an arbitrary specified wavelength, as opposed to natural (e.g., metallic) materials that have a more limited resonant response to free-space illumination. If cloaking metamaterial can be realized in practice, then semishells of this material could be used in a broad range of applications in fields such as nanoparticle chemistry, nanorheology, nanophotonics, and biophotonics. These structures would be especially useful for bioseparation by enabling selective manipulation and trapping of nanoscale biomaterial.

[1] J. B. Pendry, D. Schurig, and D. R. Smith, Science **312**, 1780 (2006).
[2] J. B. Pendry, A. J. Holden, W. J. Stewart, and I. Youngs, Phys. Rev. Lett. **76**, 4773 (1996).
[3] J. B. Pendry, A. J. Holden, D. J. Robbins, and W. J. Stewart, IEEE Trans. Microwave Theory Tech. **47**, 2075 (1999).
[4] R. A. Shelby, D. R. Smith, and S. Schultz, Science **292**, 77 (2001).
[5] A. A. Houck, J. B. Brock, and I. L. Chuang, Phys. Rev. Lett. **90**, 137401 (2003).
[6] A. Grbic and G. V. Eleftheriades, Phys. Rev. Lett. **92**, 117403 (2004).
[7] V. M. Shalaev, W. Cai, U. K. Chettiar, H.-K. Yuan, A. K. Sarychev, V. P. Drachev, and A. V. Kildishev, Opt. Lett. **30**, 3356 (2005).
[8] D. R. Smith, J. B. Pendry, and M. C. K. Wiltshire, Science **305**, 788 (2004).
[9] E. Cubukcu, K. Aydin, E. Ozbay, S. Foteinopoulou, and C. M. Soukoulis, Nature (London) **423**, 604 (2003).
[10] E. Cubukcu, K. Aydin, E. Ozbay, S. Foteinopolou, and C. M. Soukoulis, Phys. Rev. Lett. **91**, 207401 (2003).
[11] T. J. Yen, W. J. Padilla, N. Fang, D. C. Vier, D. R. Smith, J. B. Pendry, D. N. Basov, and X. Zhang, Science **303**, 1494 (2004).
[12] S. Linden, C. Enkrich, M. Wegener, J. Zhou, T. Koschny, and C. M. Soukoulis, Science **306**, 1351 (2004).
[13] D. Schurig, J. J. Mock, B. J. Justice, S. A. Cummer, J. B. Pendry, A. F. Starr, and D. R. Smith, Science **314**, 977 (2006).
[14] F. Zolla, S. Guenneau, A. Nicolet, and J. B. Pendry, Opt. Lett. **32**, 1069 (2007).
[15] D. Schurig, J. B. Pendry, and D. R. Smith, Opt. Express **14**, 9794 (2006).
[16] S. A. Cummer, B.-I. Popa, D. Schurig, D. R. Smith, and J. B. Pendry, Phys. Rev. E **74**, 036621 (2006).
[17] H. Chen and C. T. Chan, Appl. Phys. Lett. **90**, 241105 (2007).
[18] H. Chen, B.-I. Wu, B. Zhang, and J. A. Kong, Phys. Rev. Lett. **99**, 063903 (2007).
[19] B. L. Zhang, H. Chen, B.-I. Wu, and J. A. Kong, Phys. Rev. Lett. **100**, 063904 (2008).
[20] E. P. Furlani and A. Baev, J. Mod. Opt. (to be published).
[21] A. Ashkin, Proc. Natl. Acad. Sci. U.S.A. **94**, 4853 (1997).
[22] C. L. Kuyper and D. T. Chiu, Appl. Spectrosc. **56**, 295A (2002).
[23] A. Ashkin and J. M. Dziedzic, Science **235**, 1517 (1987).
[24] K. Svoboda and S. M. Block, Annu. Rev. Biophys. Biomol. Struct. **23**, 247 (1994).
[25] P. N. Prasad, *Introduction to Biophotonics* (Wiley, New York, 2003).
[26] S. Kawata and T. Tani, Opt. Lett. **21**, 1768 (1996).
[27] K. Okamoto and S. Kawata, Phys. Rev. Lett. **83**, 4534 (1999).
[28] R. Quidant, D. Petrov, and G. Badenes, Opt. Lett. **30**, 1009 (2005).
[29] M. Righini, A. S. Zelenina, C. Girard, and R. Quidant, Nat. Phys. **3**, 477 (2007).
[30] H. A. Atwater, Sci. Am. **296**, 56 (2007).
[31] E. P. Furlani, A. Baev, and P. N. Prasad, *Tech. Proc. 11th Annual NSTI Nanotech Conf.* Vol 3, edited by M. Laudon and B. Romanowitz (Nano Science and Technology Institute, Boston, 2008) Chap. 1, pp. 1–4.
[32] A. Baev, E. P. Furlani, P. N. Prasad, A. N. Grigorenko, and N. W. Roberts, J. Appl. Phys. **103**, 084316 (2008).
[33] P. C. Chaumet and M. Nieto-Vesperinas, Opt. Lett. **25**, 1065 (2000).
[34] J. I. Hage and J. M. Greenberg, Astrophys. J. **361**, 251 (1990).
[35] P. C. Chaumet, A. Rahmani, and M. Nieto-Vesperinas, Phys. Rev. B **66**, 195405 (2002).
[36] B. Zhang, H. Chen, B.-I. Wu, Y. Luo, L. Ran, and J. A. Kong, Phys. Rev. B **76**, 121101 (2007).